A multi-technique approach for studying Na triclinic and hexagonal birnessites

Hella Boumaiza, Aurélien Renard, Mbolantenaina Rakotomalala Robinson, Gwendal Kervern, Loïc Vidal, Christian Ruby, Latifa Bergaoui, Romain Coustel

A multi-technique approach for studying Na triclinic and hexagonal birnessites

Hella Boumaiza[a,b,c], Aurélien Renard[a], Mbolantenaina Rakotomalala Robinson[a], Gwendal Kervern[d], Loïc Vidal[e], Christian Ruby[a], Latifa Bergaoui[b,c] , Romain Coustel[a*]

[a] Laboratoire de Chimie Physique et Microbiologie pour les Matériaux et l'Environnement, LCPME-UMR 7564, CNRS-Université de Lorraine, 405 rue de Vandoeuvre, 54600 Villers-lès-Nancy, France

[b] Laboratoire de Chimie des Matériaux et Catalyse, Faculté des Sciences de Tunis, Université Tunis El Manar, Tunisie

[c] Département de Génie Biologique et Chimique, Institut National des Sciences Appliquées et de Technologies (INSAT), Université de Carthage, Tunis, Tunisie

[d] Laboratoire de Cristallographie, Résonance Magnétique et Modélisations, CRM2-UMR 7036, Université de Lorraine -CNRS, BP 70239 Boulevard des Aiguillettes, F 54506 Vandœuvre-lès-Nancy, France

[e] Institut de Science des Matériaux de Mulhouse (IS2M-CNRS UMR 7361-UHA), 15 rue Jean Starcky, BP 2488, 68057 Mulhouse Cedex, France

Abstract

Birnessite is a ubiquitous natural Mn oxide. This layered material is involved in a large variety of ion-exchange and redox reaction in soils and sediments. Synthetic Na-triclinic birnessite with a general formula $[Mn^{III}_{0.35}\ Mn^{IV}_{0.65}\ O_2][Na^{+}_{0.35}\ 0.7\ H_2O]$ was converted into hexagonal birnessite by acidic treatment at pH = 3.5. Both solids were fully characterized by TEM, SEM, PXRD, FTIR, Raman scattering, ^{23}Na as well as the first ^{1}H MAS NMR birnessite spectra were reported. The surfaces of both forms were fully analyzed by XPS: a particular attention was paid to the determination of the oxidation state of Mn derived from

the fitting of XPS Mn 3p or Mn $2p_{3/2}$ features. An excess of reduced Mn at the surface in comparison to the bulk materials was evidenced.

1. Introduction

Among the various manganese oxides, birnessite was found to be the most common occurring form in soils and sediments [1]. The crystal system of birnessite was shown to be either hexagonal or triclinic [2–4]. The triclinic form was initially reported as monoclinic but this symmetry was repealed by the study of Post *et al.* [4]. Hexagonal and triclinic forms are both lamellar with negatively charged layers which consist of edge-shared MnO_6 octahedra with interlayer spaces containing hydrated cations (*e.g.* Na^+, K^+, Mn^{2+}…). It is noteworthy that discrepancies appear in the nomenclature of layer type Mn oxide. In here, birnessite varieties are distinguished by the unit cell symmetry according to the recommendation of Villalobos *et al* [5].

The triclinic and hexagonal forms are essentially differentiated from each other by the origin of the charge deficit, the nature of interlayer cation and by the oxidation state of the manganese in the layers and/or interlayer. In the triclinic form (Fig. 1a), the layers have been described as an alternation of two $Mn^{IV}O_6$ rows and a $Mn^{III}O_6$ one along the *b* axis [2,6]. This structure, is actually the result of a partial substitution of Mn(IV) by Mn(III) in the MnO_6 octahedra [4,7]. The charge deficit thus created in the layers is compensated by the presence of a hydrated cation in the interlayer space (typically Na^+). In the hexagonal form (Fig. 1b), MnO_6 octahedra contains mainly manganese in the oxidation state +IV and the negatively charged layers are the result of the presence of vacancies [3]. This charge deficit is compensated by the presence of interlayer H^+ and manganese in the oxidation state +II and/or +III. The interlayer manganese ions are located above and below the vacancies [6,8].

Consequently, the relative proportions of Mn^{II}, Mn^{III} and Mn^{IV} are different in the two forms of birnessite.

Both forms of birnessite have been reported to participate in a large variety of reactions: ion exchange and sorption reaction [9–12], as well as redox reaction with heavy metals, organic or inorganic molecules [13–16]. Considering that the birnessite reactivity depends on the manganese valence state, the evaluation of the relative fractions of Mn^{II}, Mn^{III} and Mn^{IV} is of great importance. Even more, it is important to quantify these fractions at the solid surface where the reactions actually take place.

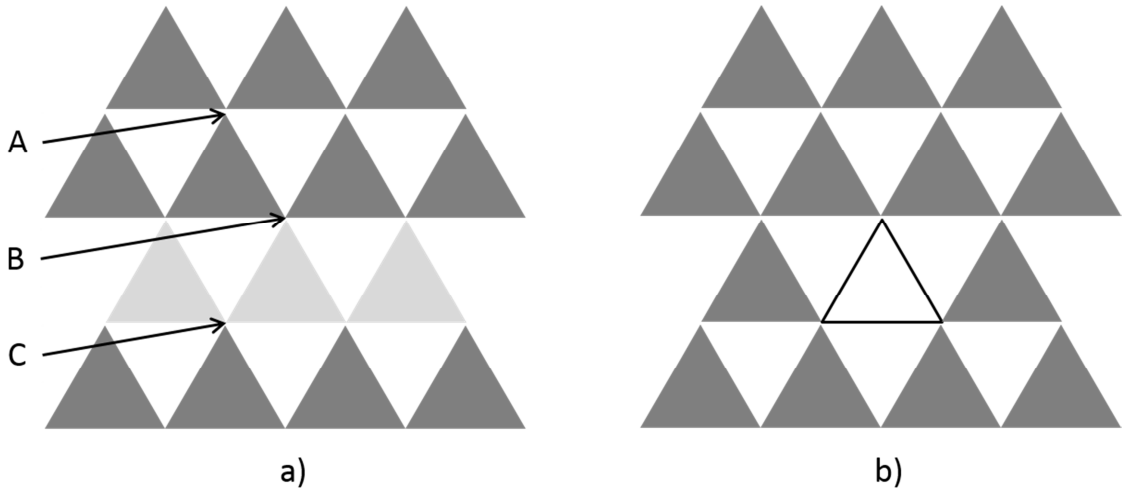

Fig. 1: Scheme of Na-Triclinic (a) and Hexagonal (b) birnessite layers (Mn^{IV} rich rows: dark grey, Mn^{III} rich rows: light grey, vacancy: empty triangle). In the triclinic form (a), the interlayer cation Na^{+} is located close to O atom that can either be coordinated to three Mn^{IV} (environment A), to two Mn^{IV} and one Mn^{III} (environment B) or to one Mn^{IV} and two Mn^{III} (environment C)

In previous studies, the manganese Average Oxidation State (AOS) in the birnessite was measured either by chemical titrations [6,17,18] or by solid characterization via Mn K- and L-edge XANES analysis [19,20]. Despite the fact that these methods provide very useful information, they are bulk techniques that do not give any information about the near-surface chemistry of the oxide where the reactions actually take place.

To this purpose, X-ray Photoelectron Spectroscopy (XPS) appears to be a preferred technique for the determination of the valence state of manganese located near the surface. There are only a few reports on the determination of Mn^{II}, Mn^{III} and Mn^{IV} relative proportions in birnessite at the surface. The earliest study used the fitting procedure of the $Mn2p_{3/2}$ XPS feature [21]. The same approach has been used by other authors [22–24] and the obtained surface-Mn AOS values were systematically lower than the bulk ones. More recently, Ilton *et al.*[25] discussed the Mn AOS determination through $Mn2p_{3/2}$, Mn3s and Mn3p lines analysis. This study raised some doubts about the use of Mn3s multiplet splitting. The $Mn2p_{3/2}$ peak shape was also suspected to be too sensitive to Mn bonding environment. Then, the authors recommended a method based on Mn3p line decomposition.

When submitted to an acidic treatment, the triclinic birnessite undergoes a symmetry conversion to hexagonal [3,6,8]. Several solid characterization techniques were recently reported in order to understand both birnessite structures: Fourier Infrared Spectroscopy (FTIR) [26,27], Raman scattering [28], Mn K and L-edge extended X-ray absorption fine structure (EXAFS) [29], ^{23}Na Magic Angle spinning Nuclear Magnetic Resonance (MAS NMR) [30] or XPS [25]. However, as far as we know, conversion from triclinic to hexagonal form was not yet investigated by a multi-technique approach.

The main goals of this study are thus (i) to probe the changes of triclinic birnessite placed at pH 3.5 by monitoring both the liquid and, especially, solid properties by a comprehensive set of physical chemistry methods: Transmission electron microscopy (TEM), Scanning Electron microscopy (SEM), powder X-ray diffraction (PXRD), FTIR, Raman scattering, ^{23}Na and ^{1}H MAS NMR and XPS, (ii) to discuss the XPS use for the Mn AOS assessment at the near-surface of different studied solids.

2. Materials and methods

2.1. Chemicals

All chemicals were purchased from Sigma-Aldrich. Manganese (II) chloride tetrahydrate ($MnCl_2 \cdot 4H_2O$, ACS reagent, ≥98%), sodium permanganate monohydrate ($NaMnO_4 \cdot H_2O$, ACS reagent ≥97%) and sodium hydroxide (NaOH, BioXtra, ≥98% pellets anhydrous) were used for birnessite's synthesis. Hydrochloric acid (ACS reagent, 37%) was used to convert Na triclinic birnessite into hexagonal one in acidic medium. Mohr salt ($(NH_4)_2Fe(SO_4)_2 \cdot 6H_2O$, ACS reagent, 99%), sodium pyrophosphate dibasic ($Na_2H_2P_2O_7$, practical grade) and potassium permanganate ($KMnO_4$, ACS reagent, ≥99.0%) were used to measure the Mn AOS in birnessite. Hexaamminecobalt(III) chloride ($[Co(NH_3)_6]Cl_3$, 99%) was used for the determination of the Cation Exchange Capacity (CEC) of the birnessite. Hydroxylamine hydrochloride (NH_3OHCl, ACS reagent, ≥ 96 %) was used for the complete digestion of birnessite before ICP-AES analysis.

2.2. Synthesis of birnessite

The triclinic birnessite was obtained following the alkaline method of synthesis proposed by Boumaiza *et al.* [22] in which 125 mL of NaOH (8.8 mol L^{-1}) is added dropwise during 2 hours to a mixture of 250 mL of $NaMnO_4$ (0.1 mol L^{-1}) and 125 mL of $MnCl_2$ (0.6 mol L^{-1}). The mixture is then kept under stirring during an additional 30 minutes, aged at 60 °C during 14 h, washed until the supernatant pH is 9 – 10 and dried at 60 °C for 16 hours. The obtained product consisted on triclinic Na-birnessite with a general formula $[Mn^{III}_{0.35}\,Mn^{IV}_{0.65}\,O_2][Na^{+}_{0.35,}\,0.7\,H_2O]$. For this triclinic birnessite, the Mn AOS is equal to 3.65 and the CEC is equal to 2.3 meq g^{-1}.

The hexagonal birnessite was obtained from the transformation of triclinic Na-birnessite in acid solution: Na-birnessite suspension (6 g L^{-1}) was maintained at pH 3.5±0.1 throughout the

experiment using a computer-controlled titrator (736 GP Titrino, Metrohm) by adding hydrochloric acid solution (0.2 mol L-1, for a total HCl amount of about 4 mmol). Aliquots were collected at different contact times and filtered through 0.22 µm syringe filter. After 24 h of contact time, the remaining birnessite was collected for solid state characterizations. In sake of comparison, a similar experiment without pH stabilization was also performed (pH = 10).

2.3. Characterization techniques

In order to establish the chemical formula of the Na-birnessite, the Na and Mn contents were measured by Inductive Coupled Atomic Emission Spectroscopy ICP-AES (JobinYvon-Horiba, Ultima) after complete digestion of about 5 mg of solid in NH_3OHCl (0.7 mol L^{-1}, pH = 1.9). The water content was determined by thermogravimetric analysis (LABSYS Evo Setaram Instrument) under dry inert gas flow. The sample was heated from room temperature to 800 °C (heating rate: 10 °C min^{-1}). The interlayer water was evaluated based on the endothermic curve between 70 and 250 °C.

The CEC was determined using a Cobalt-hexaamine method [31] by putting 150 mg of birnessite in 20 mL of $Co(NH_3)_6Cl_3$ (16.67 mol L^{-1}). The mixture was then shaken for 2 hours, without temperature regulation, and microfiltered. The measurement of the cobalt-hexaamine concentrations before and after reaction time was performed by UV-visible analysis at 472 nm using an Agilent Cary 60 spectrophotometer.

The Mn AOS in birnessite samples was measured by a potentiometric titration using Mohr salt, potassium permanganate and sodium pyrophosphate dibasic. This method is based on the work of Lingane and Karplus [17] and Vetter and Jaeger [18,32].

After acidic treatment of Na-birnessite, Mn content in the supernatant was also measured by ICP-AES (JobinYvon-Horiba, Ultima).

TEM images were obtained by using a Philips CM 200 (accelerating voltage 200 kV). SEM images were obtained using a JEOL JCM-6000 microscope (accelerating voltage 15 kV).

PXRD was performed at room temperature by using a Panalytical X'Pert Pro diffractometer and an X′Celerator as a detector. Data collection were carried out using 0.02 rad Soller slits, programmable divergence and antiscatter slits, the irradiated area was fixed to 10x10 mm. The PXRD patterns were recorded using $CuK_{\alpha 1}$ radiation (λ=0.15406 nm). Data collection was carried out in the scattering angle range 5-70° with a 0.0167° step over 2 hours.

FTIR analysis was performed using a Bruker Vertex 70v equipped with a DLaTGS detector in transmission mode using KBr pellets containing 2–5 mg of sample. For each sample, 100 scans were collected in the 4000 – 220 cm^{-1} range with 4 cm^{-1} resolution. The KBr spectrum was also recorded at the same conditions and was subtracted from the sample spectra.

Raman scattering measurements were performed on a Renishaw inVia Qontor spectrometer equipped with a Leica confocal microscope and using a Nd:YAG laser source emitting at 532 nm. The laser was focused on the sample by a ×100 objective. The laser power was kept at 0.05 mW to avoid any heating effect. Each scan consists of 50 accumulations of 10 seconds.

X-ray photoelectron spectra were recorded on a KRATOS Axis Ultra X-ray photoelectron KRATOS Axis Ultra DLD spectrometer equipped with a monochromated Al Kα source (hυ = 1486.6 eV, spot size 0.7 mm×0.3 mm). The samples were pressed onto a Cu tape fixed on a sample holder and introduced into the spectrometer. The detector is a hemispherical analyzer at an electron emission angle of 90° and pass energy of 160 eV (survey spectra) or 20 eV (high resolution spectra). For the high-resolution spectra, the overall energy resolution, resulting from monochromator and electron analyzer bandwidths, was better than 800 meV. Charge correction was carried out using the C1s core line, setting adventitious carbon signal to 284.6 eV. Na1s and O1s spectra were decomposed using Gaussian peaks after using Shirley method of background subtraction.

All ^{1}H (reference adamantane 1.8 ppm) and ^{23}Na (reference NaCl 0 ppm) NMR spectra were realized on a 7.05 T Bruker AVANCE III spectrometer equipped with a 4 mm CPMAS probe, under 12.5 kHz MAS, direct acquisition and no proton decoupling. The ^{23}Na spectra were acquired after a 1 second delay and 1 μs hard pulse, the proton spectra were acquired after a 10 ms delay and 1 μs hard pulse. The proton spectra were acquired with a presaturation prior to acquisition, as well as a rotor synchronized echo in order to get rid of the slow relaxing signals (probe background signal, free water).

3. Results

3.1. Birnessite solubility in acidic medium

When submitted to an acidic treatment at pH = 3.5 during 24 h, triclinic Na-birnessite undergoes a change of symmetry to hexagonal accompanied by Mn release in the solution that has been monitored during time (Fig. 2). This soluble Mn is assumed to be Mn^{2+} since Mn^{III} and Mn^{IV} are essentially stable in solid-phase. In fact, the Mn^{IV} complexes, even in coordinated state, are hydrolyzed to form MnO_2 and, in the absence of complexing agents, Mn^{III} disproportionates to form Mn^{II} and Mn^{IV} [33,34]. The evolution of the Mn^{2+} concentration over time (Fig. 2) is characterized by two stages. The first step is an increase of the Mn^{2+} to a maximum of 1.6 mmol L^{-1} after 30 minutes. The second step is the slow decrease in concentration up to 1.3 mmol L^{-1} at 180 minutes and stabilization around this value for up to 24 hours of reaction. At this pH, the amount of Mn^{2+} released in the solution represents 3% of the total Mn while at pH 10, no Mn^{2+} was detected in the supernatant.

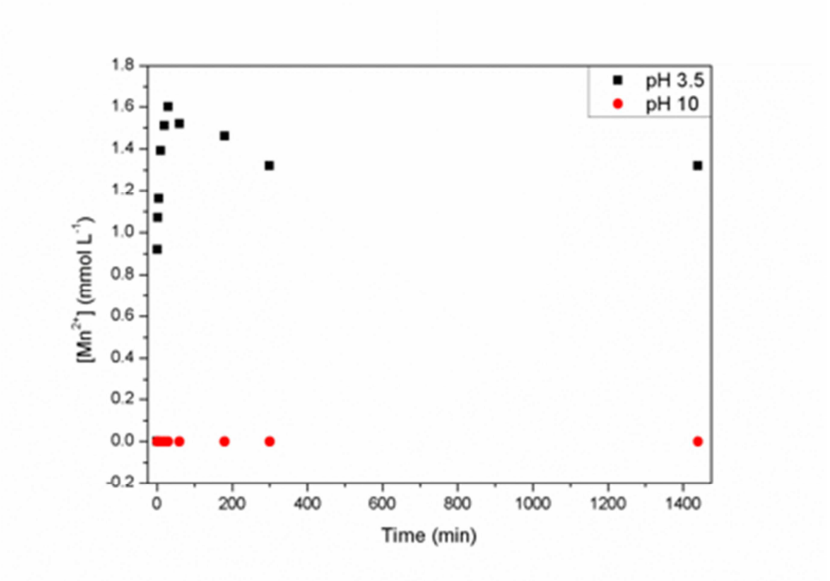

Fig. 2. Evolution of soluble Mn concentration in triclinic birnessite suspension as function of time at pH 3.5 and 10 ([Na-bir] = 6 g L^{-1}, T = 25 °C).

3.2. Solid analysis

The TEM images of as prepared Na-birnessite and after acidic treatment (Fig. 3a and 3.b) highlights a rectangular shaped particles morphology similar to what has been previously observed [5,35,36]. Moreover, both samples present a lamellar structure with an appearance of well aligned layers having an interlayer spacing of ca. 0.6 – 0.7 nm for hexagonal birnessite and ca. 0.5 – 0.6 nm for triclinic birnessite. These values, less important than the ones measured by XRD analysis (ca. 0.7 nm), are probably the result of a loss in water molecules from the interlayer space when sample is under vacuum (5.10^{-5} Pa) during the TEM analysis [37]. SEM images (Fig. 3) show that both samples consist of aggregates of layered particles in the range size of few µm. The morphology of birnessite seems to be not significantly affected by acidic treatment.

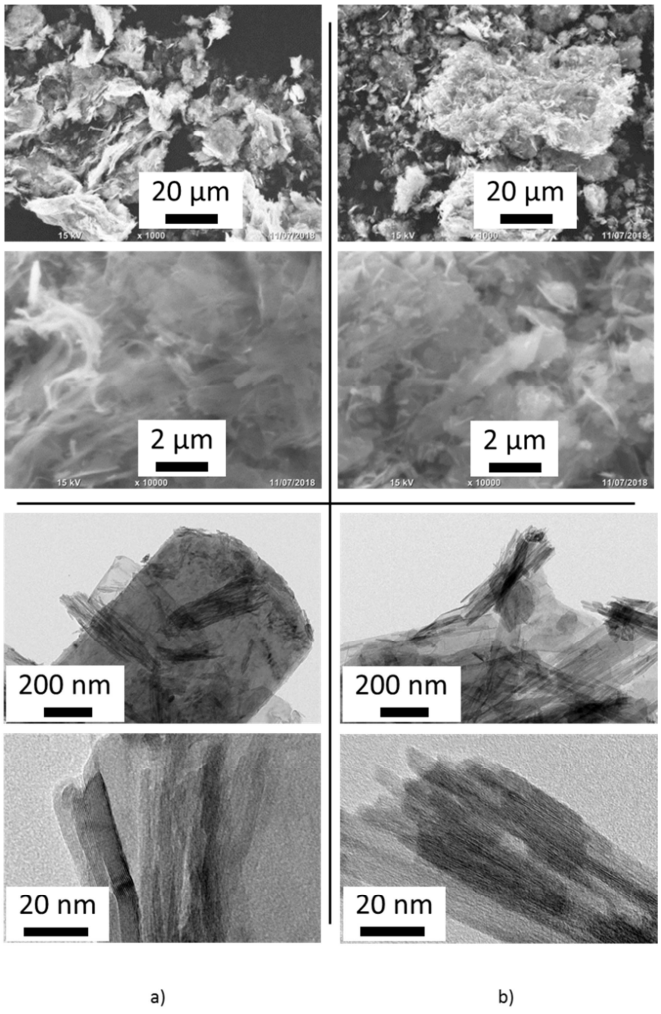

Fig. 3. TEM (lower panel) and SEM (upper panel) images of a) as-prepared triclinic Na-birnessite and b) after acidic treatment (pH = 3.5, [Na-birnessite] = 6 g L^{-1}, T = 25 °C, reaction time = 24 h).

- *PXRD characterizations*

Figure 4 presents the PXRD pattern of the prepared Na-birnessite before (Fig. 4.a) and after acidic treatment (pH = 3.5 during 24 h, Fig. 4.b). The diffractogram of the initial birnessite corresponds to a triclinic Na-birnessite (PDF 00-043-1456) with two main diffraction peaks at 7.13 and 3.57 Å assigned to the basal reflection 001 and 002, respectively. A series of additional peaks are displayed for the 2θ range from 30 to 70°, assigned to intralayer reflections. The program GSAS/EXGUI [38,39] was used for the Le Bail extraction in space group $P\bar{1}$. Only the cell dimensions, parameters of the pseudo-Voigt profile shape function

and the zero shift were refined (Le Bail extraction is given in Fig. S1). Obtained lattice constants are: a = 2.954(2) Å, b = 2.955(2) Å, c = 7.330(2) Å, α = 78.76(4)°, β = 101.84(4)° and γ = 122.34(2)° (uncertainty was taken to be 3 times the standard deviation derived from Le Bail extraction). These parameters are in fair agreement with those proposed by Lanson *et al*. [2]: a = 2.9513(4) Å, b = 2.9547(4) Å, c = 7.334(1) Å, α = 78.72(2)°, β = 101.79(1)° and γ = 122.33(1)°. All PXRD peaks (Fig. 4.a) were indexed on the basis of this triclinic unit cell.

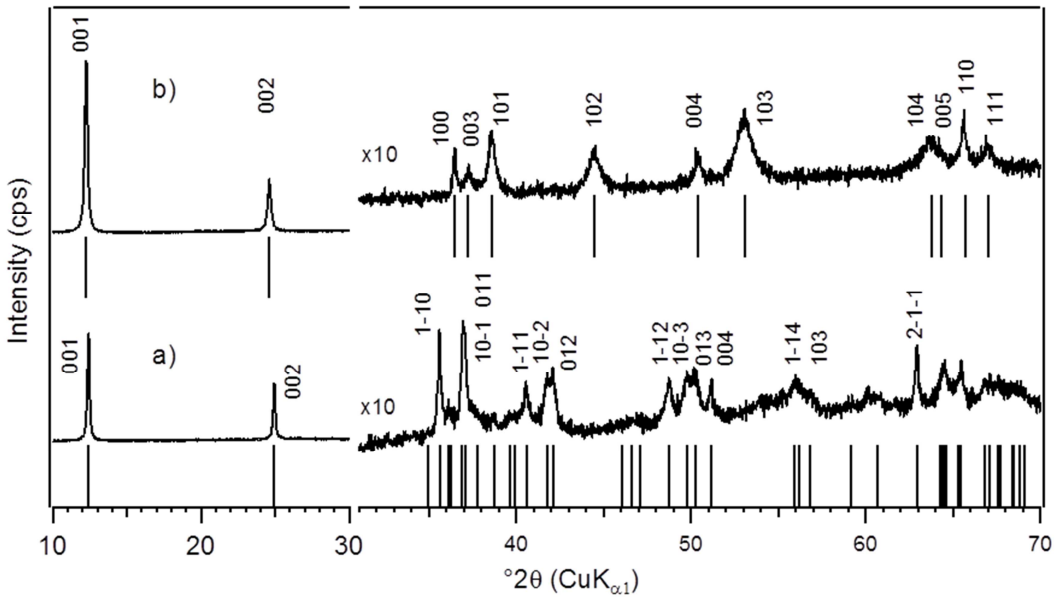

Fig. 4. PXRD patterns of a) as-prepared triclinic Na-birnessite and b) after conversion into hexagonal birnessite by acidic treatment (pH = 3.5, [Na-birnessite] = 6 g L^{-1}, T = 25 °C, reaction time = 24 h).

After acidic treatment, basal reflections shifted slightly toward lower 2θ values which correspond henceforth to the distances 7.24 and 3.62 Å. For 2θ range from 30 to 70°, the initial reflections of the triclinic form collapsed and the product maintained at pH 3.5 during 24 h revealed other reflection peaks corresponding to hexagonal birnessite [3,6]. The measurements of lattice parameters using the Le Bail method gave a = 2.844(2) Å and c = 7.238(3) Å (uncertainty was taken to be 3 times the standard deviation derived from Le Bail extraction, see Fig. S1).

- *FTIR and Raman scattering characterizations*

The solids were further characterized by FTIR analysis (Fig. 5A) and the obtained band positions are compared with reported existing studies on Table 1. Both triclinic Na-birnessite and hexagonal birnessite show strong absorption bands in the 220 – 700 cm^{-1} range. These bands are assigned to Mn-O lattice vibration in good agreement with the reported spectra of triclinic [27,40–42] and hexagonal birnessite [26,27].

Triclinic Na-birnessite is characterized by the presence of bands located at 245, 360, 417, 478, 513 and 636 cm^{-1} and by a shoulder at 550 cm^{-1}. As expected from its higher degree of symmetry, the FTIR spectrum of hexagonal birnessite presents a reduced number of absorption bands located at 341, 426, 496 and 658 cm^{-1}. These band positions are in fair agreement with previous experimental results [26,27] in the 400 – 700 cm^{-1} range (see Table 1). On the basis of DFT calculations where birnessite was modeled with a cluster approach, these authors indicated that clear band assignment remained delicate due to strong overlap of Mn-O vibration modes below 700 cm^{-1}.

Interestingly, measurement in the far infrared range allow the identification of additional absorption band at 245 and 360 cm^{-1} for triclinic Na-birnessite and 341 cm^{-1} for hexagonal birnessite. DFT calculations predicted absorption band below 400 cm^{-1} for hexagonal birnessite but no absorption band was predicted for triclinic birnessite in this range [26,27]. Actually, these calculations were based on $Mn_xO_yH_z$ clusters without considering Na^+ species in the interlayer region. Then, one may suggest that these extra bands could be associated to cation vibrations.

Additional vibration modes appear at higher wavenumber. Interlayer water gives rise to absorption band in the regions of ~1400 – 1650 cm^{-1} and 3000 – 3600 cm^{-1} corresponding to bending and stretching modes. In both regions, triclinic Na-birnessite presents narrower bands

than what is observed for hexagonal form. This could be attributed to higher degree of order of the water molecules in the interlayer region and/or to higher degree of crystallinity of the whole material. The latter point is supported by PXRD results where the triclinic form presents sharper diffraction pattern. Lastly, no feature is observed in the range of 950 – 1200 cm^{-1}, which is generally associated with the Mn-O-H bending mode [43,44]. Then, significant amount of MnOOH as well as Mn-OH moieties in birnessite samples can be ruled out.

The Raman scattering spectra of triclinic Na-birnessite and hexagonal birnessite shown in Figure 5B are compared to reported existing studies on Table 1. The position as well as the relative intensities of the Raman bands are in good agreement with the reported spectra of birnessites [45,46].

Indeed, both spectra display characteristic manganese oxide Raman fingerprints in the range from 400 to 700 cm^{-1} showing: 1) a strong band between 635 and 650 cm^{-1} that can be attributed to the Mn-O symmetric stretching vibration ν_2(Mn–O) of MnO_6 group, 2) a band around 575 and 587 cm^{-1} corresponding to the Mn-O stretching vibration ν_3(Mn–O) in the basal plane of [MnO_6] sheets [45], 3) additional bands with weaker intensities displayed at 509, 485 and 405 cm^{-1} for the triclinic symmetry, and around 500 and 387 cm^{-1} for the hexagonal form that are attributed to Mn–O–Mn bending vibration. Due to its higher symmetry, the hexagonal form presents less characteristic bands than the triclinic form [47]. An additional band is observed in the Raman spectrum of the triclinic Na-birnessite located at 279 cm^{-1}. This band has been previously attributed to the weak bond of the intercalated Na^+ between MnO_6 layers [46]. Finally, an unassigned additional band located at 610 cm^{-1} appears in the hexagonal birnessite spectrum. Previous studies have shown that the appearance of this Raman band is strongly dependent on the synthesis parameters [48].

Then, in complete agreement with PXRD results, FTIR and Raman scattering spectra confirm that, triclinic Na-birnessite is converted into hexagonal birnessite when maintained at pH = 3.5 during 24 h, as it has been previously observed [3,6,8].

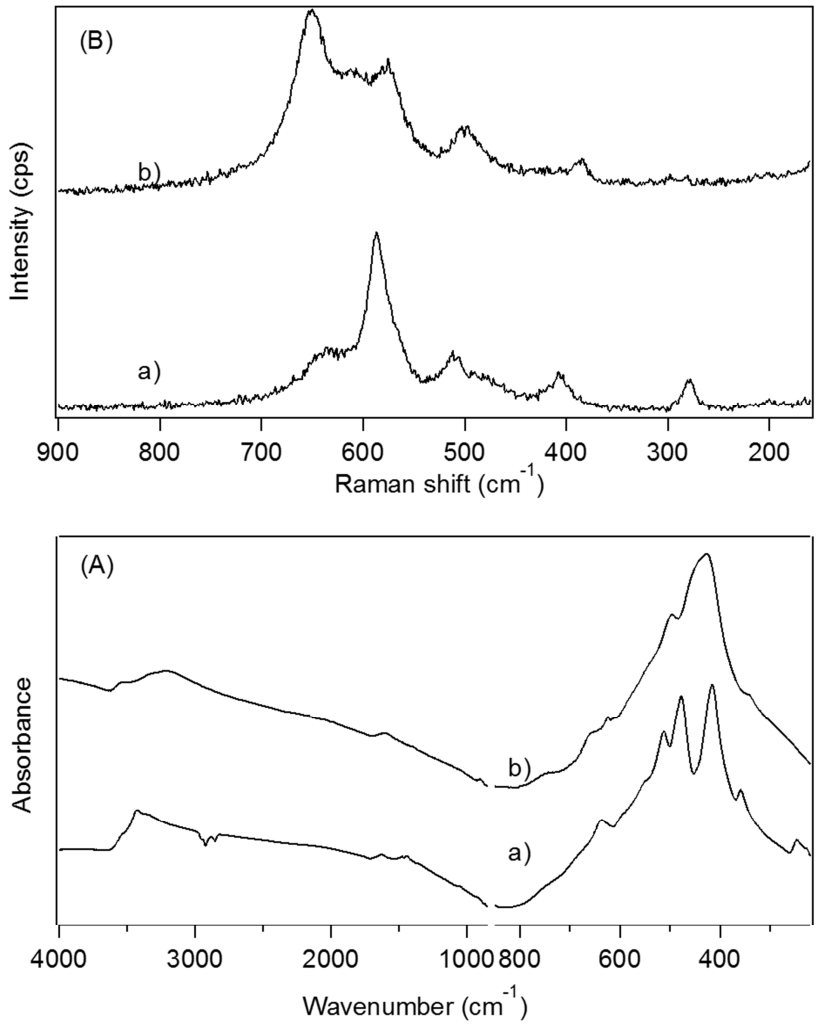

Fig. 5. FTIR (A) and Raman scattering (B) spectra of a) as-prepared triclinic Na-birnessite and b) after conversion into hexagonal birnessite by acidic treatment (pH = 3.5, [Na-bir] = 6 g L^{-1}, T = 25 °C, reaction time = 24 h).

Table 1: FTIR and Raman band location (cm^{-1}) and attribution for triclinic Na-birnessite and hexagonal birnessite in comparison to previous studies (the reported FTIR bands are based on ref. [26,27] while the reported Raman bands are based on ref. [45,46])

	FTIR band position (cm^{-1})			Raman band position (cm^{-1})		
	This study	Previous studies		This study	Previous studies	
Triclinic Na-birnessite	245		interlayer Na^+ vibrations	200	195	
	360			279	281	interlayer Na^+ vibrations
	417	418	Mn-O lattice vibrations	405	408	Mn-O-Mn bend.
	478	478		485	480	
	513	511		509	509	
				587	584	ν_3: Mn-O stretch. in the basal plane of $[MnO_6]$ sheets
	636	639		635	637	ν_2: Mn-O symm. stretch. of MnO_6
Hexagonal birnessite	341		Mn-O lattice vibrations		296	*
				387		Mn-O-Mn bend.
	426	440				
	496	494		500	506	
				575	575	ν_3: Mn-O stretch. in the basal plane of $[MnO_6]$ sheets
				610		*
	658	659		650	646	ν_2: Mn-O symm. stretch. of MnO_6
					730	*

*Unassigned

- *^{23}Na and ^{1}H NMR analysis*

The ^{23}Na MAS NMR spectra of triclinic and hexagonal birnessite are presented in figure 6-A. The spectrum of triclinic Na-birnessite seems quite similar to those shown in a previous study [30]. The spectrum displays 3 signals corresponding to different chemical environments within the triclinic birnessite with isotropic shifts of 435, 376 and 329 ppm respectively (crystalline NaCl has been used to set the 0 ppm signal). The other observed peaks in the spectrum correspond to the spinning side bands due to a strong chemical shift anisotropy (CSA) due to hyperfine interaction with the unpaired electrons in Mn^{III} and Mn^{IV} as well as first order quadrupolar coupling. Those signals are broadened by magnetic field distribution due to field inhomogeneity as well as second order quadrupolar interaction. According to

Lanson *et al.* [3] Na-birnessite layer is formed of one row of $Mn^{III}O_6$ octahedra separated by two rows of $Mn^{IV}O_6$ octahedra. Each Na^+ ion is bonded to the oxygen layer, then coordinated to three $Mn^{III/IV}$ ions via the bonded oxygen. Aldi *et al.* [30] attributed the three ^{23}Na peaks to different chemical environments where Na^+ ion was coordinated to i) three Mn^{IV} (environment A, see fig. 1), ii) two Mn^{IV} and one Mn^{III} (environment B) or iii) one Mn^{IV} and two Mn^{III} (environment C). Following Aldi *et al*'s work [30], we assume that these environments correspond to the peaks at i) 435, ii) 376 and iii) 329 ppm respectively. This assignment is validated despite the slight differences in isotropic shifts between our observations and those made in Aldi *et al*'s work [30]. Indeed, since the shifts that are presented in this paper are strongly field-dependent, a simple extrapolation shows that the assignment proposed in here falls close to the one observed in Aldi *et al*'s work. In consequence, it appears that Na^+ ions occupied A, B and C sites thus suggesting that the synthesis method used in this study provides birnessite with cation disorder in the interlayer space.

Lastly, there is an additional, relatively narrow and weak signal at -11 ppm that corresponds to an unidentified impurity that does not undergo the effects of hyperfine interaction and may thus not be inside the material. Given its limited NMR shift, this signal is compatible with traces of sodium salt. There should be a counter anion associated with that Na^+. As XPS did not show the presence of Cl^-, SO_4^{2-}, NO_3^- (see hereafter), one can assume this sodium salt to be NaOH. Moreover, since hydrated NaOH is expected to be not crystalized, this assumption is also consistent with PXRD result.

All ^{23}Na signals disappear completely in the hexagonal birnessite, thus confirming the total sodium removal when the triclinic Na-birnessite turns to a hexagonal one.

The ^1H MAS NMR spectra of triclinic and hexagonal birnessite are presented in figure 6-B. Both spectra show two signals. The first one has an isotropic shift close to 0 ppm. It presents

very little CSA and has the same intensity in both spectra. This signal could be assigned to water molecule physisorbed at the surface [49] or to a background signal that remains from the presaturation. The second signal, also present in both spectra but with different intensity this time, presents a very strong CSA. This signal is weaker with a shift of 13 ppm for the hexagonal birnessite with respect to the triclinic one. The very large observed CSA is due to the hyperfine coupling with the manganese unpaired electrons. This indicates the close proximity of those protons to the metallic center. These protons probably belong to hydration water located in the interlayer space. Since the triclinic birnessite contains more water than the hexagonal one [3], the intensity of the related signal is larger for the triclinic form.

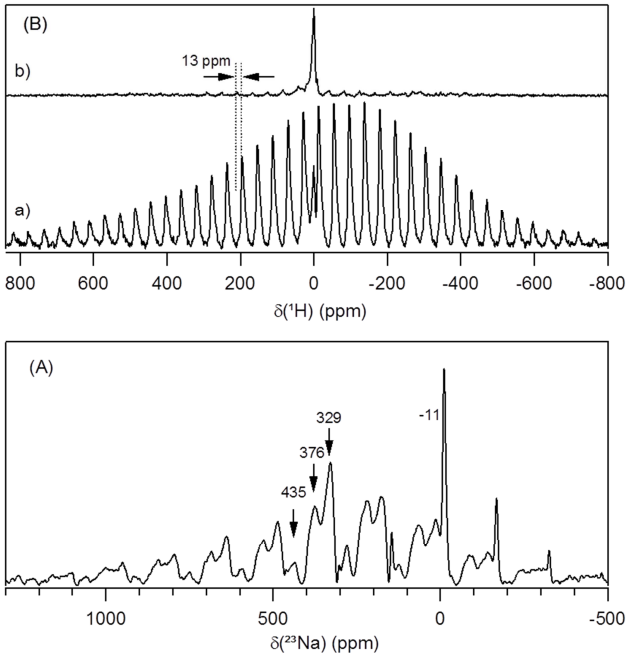

Fig. 6. (A) ^{23}Na solid-state MAS NMR of as-prepared triclinic Na-birnessite, the center bands on the spectra are identified by the arrows above them and the corresponding isotropic shifts. All the other peaks are spinning sidebands. (B) ^{1}H solid-state MAS NMR spectra of a) as-prepared triclinic Na-birnessite and b) after conversion into hexagonal birnessite by acidic treatment (pH = 3.5, [Na-bir] = 6 g L^{-1}, T = 25 °C, reaction time = 24 h).

Furthermore, the PXRD study concluded that the thickness of the interlayer space is smaller for the triclinic Na-birnessite which suggests that the water molecules are closer to the Mn

oxide layers for the triclinic birnessite when compared to hexagonal variety. This observation may explain the difference in the CSA and the 13 ppm shift between the two signals. The shift can also be explained by the chemical environment of the nuclear probe; $H_2O^{\cdots}Na^+$ for Na-birnessite *vs* $H_2O^{\cdots}H^+$ for the hexagonal form.

- *XPS analysis*

Surface properties of Na-birnessite and hexagonal birnessite were examined by XPS. Overview XPS spectra (Fig. 7.a and 7.b) show core-level photoelectron peaks at ~50 eV (Mn3p), ~285 eV (C1s), ~530 eV (O1s), ~642 eV ($Mn2p_{3/2}$), ~654 eV ($Mn2p_{1/2}$), ~770 eV (Mn2s) and ~1071 eV (Na1s). The C1s peak should be attributed to atmospheric hydrocarbon contamination of the birnessite surface before introduction into the XPS chamber.

The Na1s spectrum of Na-birnessite presents one peak located at 1070.7 eV (FWHM = 1.5 eV) corresponding to one chemical environment of Na atom at the surface. Na1s peak is no more observed for the hexagonal form. This disappearance indicates a complete release of Na ions observed at the surface from the solid at pH = 3.5. This is in line with the triclinic to hexagonal conversion observed by FTIR, Raman, PXRD as well as NMR analyses. On the contrary to XPS, various Na environments in Na-triclinic birnessite can be distinguished by NMR measurements. This should be mainly attributed to the fact that the position of XPS feature essentially depends on the oxidation state of the atom while NMR displacement also depends on the local chemical environment (packing, hyperfine interactions).

The O1s spectra of both samples present a maximum at 529.6 eV and a broad shoulder at higher binding energy. The low binding energy peak corresponds to lattice oxygen (O^{2-}). The medium binding energy peaks (531 eV) are assigned to O^- and OH groups. The higher binding energy peak (533 eV) is attributed to adsorbed water [50,51]. For both samples O^- and

OH contributions represent more than 20 % of O1s spectrum. This result is in line with a high amount of surface defect.

Particular attention was paid to $Mn2p_{3/2}$ and Mn3p peaks from which it has been claimed that the valence state of Mn can be extracted [21,25]. Following these studies, the $Mn2p_{3/2}$ and Mn3p peaks were then decomposed and the results were compared to each other and to the bulk analysis in order to determine the accuracy of each method. The corresponding results are given in Figure 7 and Table 2 while the fitting parameters are given in supplementary materials (see Table S1).

The $Mn2p_{3/2}$ spectrum of Na-birnessite (Fig. 7.c) is centered at 642 eV with shoulders at 641 eV and 643 eV, as expected for Mn^{III}-Mn^{IV} birnessite [22]. Similar but widened feature is observed for hexagonal birnessite (Fig. 7.d) with additional contribution at 639 eV. This low binding energy component is attributed to Mn^{II} contribution [21,25].

Based on the earlier work of Gupta and Ken [52], Nesbitt and Banerjee [21] have proposed a method to isolate the Mn^{II}, Mn^{III} and Mn^{IV} contributions of $Mn2p_{3/2}$ peak in birnessite. According to calculations of multiplet structure core p-vacancy levels, each valence state contribution was modeled as a multiplet whose parameters were derived from ab-initio calculations. $Mn2p_{3/2}$ spectra of triclinic Na-birnessite and hexagonal birnessite were fitted following the recommendations of Nesbitt and Banerjee [21]. This analysis confirms that Na-birnessite presents only Mn^{III} and Mn^{IV} while hexagonal birnessite presents an additional Mn^{II} component representing a relative area of 7±2 %. It also appears that Mn^{III} content decreases while Mn^{IV} content increases after acidic treatment, in line with the mechanism proposed in previous studies [3,6,8].

Recently, Ilton *et al.* [25] claimed that a more reliable evaluation of Mn^{II}, Mn^{III} and Mn^{IV} distribution on the surface can be obtained from the Mn3p signal. Actually, the Mn3p peaks

for triclinic Na-birnessite and hexagonal birnessite are located at 50 eV with a shoulder at 48 eV. These authors proposed an empirical approach where each valence state contribution was described as a multiplet whose shape is experimentally determined from XPS measurement on monovalent Mn oxide (MnO, MnOOH and MnO_2). Following the same Mn3p fitting procedure, the obtained results indicates that Mn^{II} appears after acid treatment while Mn^{III} and Mn^{IV} content decreases and increases respectively, as observed when using $Mn2p_{3/2}$ spectra.

The Mn^{II}, Mn^{III} and Mn^{IV} distribution on the surface obtained from the $Mn2p_{3/2}$ and Mn3p peaks fitting along with the Mn AOS of the bulk given by potentiometric titration are summarized in Table 2. Our results show that, regardless of the fitted Mn peak, surface analysis by XPS give the same value of Mn AOS, unlike what has been previously observed in Ilton *et al.* work [25]. Indeed, the Mn AOS of triclinic form is found equal to 3.43±0.05 and 3.47±0.05 according to $Mn2p_{3/2}$ and Mn3p fittings respectively while it was equal to 3.60±0.08 and 3.56±0.06 according to $Mn2p_{3/2}$ and Mn3p fittings respectively for the hexagonal form. These values derived from surface analysis are significantly lower than the bulk values of 3.65±0.02 and 4.00±0.02 obtained for the triclinic and hexagonal forms respectively. Actually XPS is a surface sensitive technique that only probes the first few nanometers of birnessite particles whose size are in the range of µm (determined from SEM measurements). These results support Mn AOS gradient between surface and bulk.

It should be noted that PXRD did not evidence any Mn^{II} salt along with hexagonal birnessite. Accordingly, XPS measurements did not evidence any counter-ion (e.g. no chloride) likely to form Mn^{II} salt. Then, it comes that Mn^{II} content is intimately associated to hexagonal birnessite phase.

In brief, following the approaches of Nesbitt *et al*. [21] and Ilton *et al*. [25], we showed that Na-triclinic birnessite conversion to hexagonal one leads to (i) Mn^{II} formation at the solid surface as well as (ii) $\%Mn^{III}$ decrease and $\%Mn^{IV}$ increase. Moreover, unlike what has been

claimed in the study of Ilton *et al.*, [25] (iii) Mn average oxidation state at the surface given by these two methods are essentially similar.

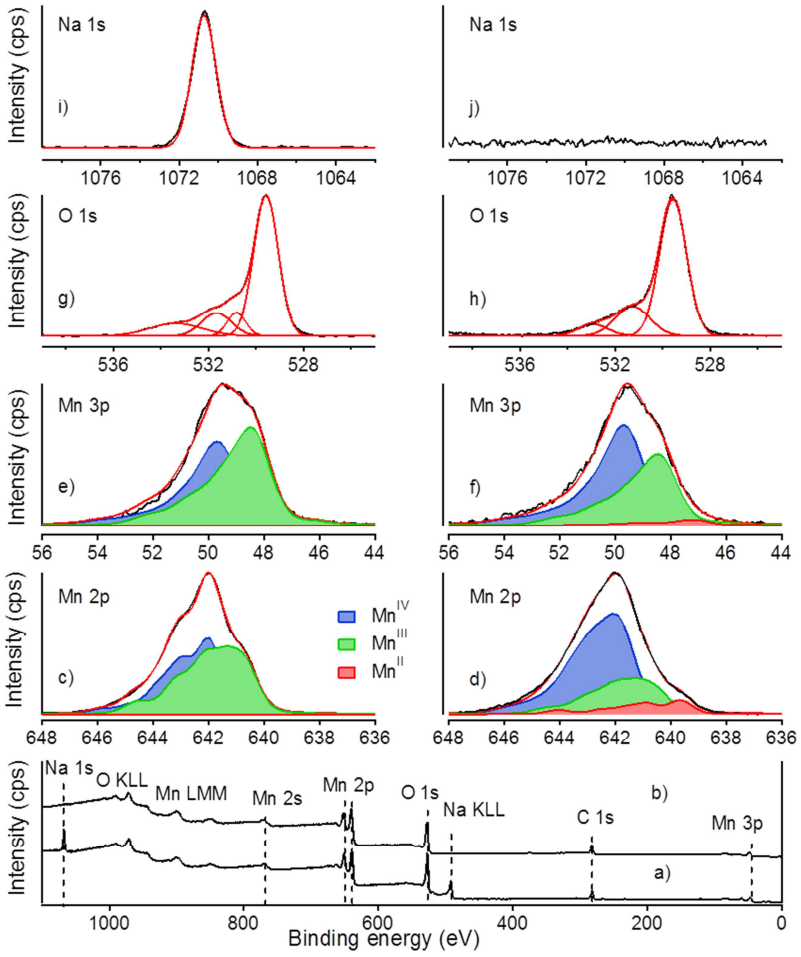

Fig.7. Survey, $Mn2p_{3/2}$, Mn3p, O1s and Na1s XPS spectra of the triclinic Na-birnessite (a, c, e, g and i) and the hexagonal birnessite (b, d, f, h and j) (pH = 3.5, [Na-bir] = 6 g L^{-1}, T = 25 °C, reaction time = 24 h).

Table 2: Mn^{II}, Mn^{III} and Mn^{IV} distribution on the surface derived from XPS measurements compared to AOS of the bulk.

	Triclinic Na-birnessite		Hexagonal birnessite	
	$Mn2p_{3/2}$ fitting	Mn3p fitting	$Mn2p_{3/2}$ fitting	Mn3p fitting
Mn^{II} (%)	-	-	7±2	2±1
Mn^{III} (%)	57±6	53±5	26±4	40±4
Mn^{IV} (%)	43±5	47±5	67±6	58±5
$AOS_{surface}$	3.43±0.05	3.47±0.05	3.60±0.08	3.56±0.06
AOS_{bulk}	3.65±0.02		4.00±0.02	

4. Discussion

As evidenced by PXRD, FTIR and Raman scattering results, when dispersed during 24 h in an acidic aqueous solution (pH = 3.5), triclinic Na-birnessite changes its symmetry to hexagonal. This structural transformation is accompanied by complete Na removal form the solid, as confirmed by XPS and NMR measurements. This is in line with earlier works in which the symmetry conversion was studied by different techniques [3,6,8].

At pH 3.5, the amount of Mn^{2+} released in the solution is characterized by two phases: an increase within the initial 30 minutes up to 1.6 mmol L^{-1} and then a decrease to stabilize at 1.3 mmol L^{-1} at 24 h (Fig. 2). This result can be brought into connection with the previous observation showing that the reaction of triclinic birnessite placed in an acidic medium could be explained by a two steps reaction. The first step corresponds to the partial disproportionation of Mn^{III} contained in the layers into Mn^{II} and Mn^{IV}. Mn^{II} is then dissolved in acidic medium leading to vacancies formation in the layers following reaction:

$$2Mn^{3+}_{(layer)} \rightarrow Mn^{4+}_{(layer)} + Mn^{2+}_{(layer)} \rightarrow Mn^{4+}_{(layer)} + \text{vacancy} + Mn^{2+}_{(aq)} \quad (1)$$

In a second step, a part of the dissolved Mn^{2+} re-adsorbs on the surface, above and below vacancies, resulting in the diminution of the amount of aqueous Mn^{2+} [6,8]. According to this mechanism, if final $Mn^{2+}_{(aq)}$ represents reduced fraction of total Mn, the AOS of the solid would scarcely evolve but these authors did not evidence any AOS change (~3.6). At this point, it should be highlighted that Silvester *et al.* [6] preserve the reactive medium from further oxidation with Ar bubbling.

In here, while birnessite's conversion was performed without any protection against oxygen, a significant increase of the Mn AOS was evidenced both in the bulk (from 3.65 to 4.00) and at the surface (from 3.4 to 3.6). It is interesting to note that soluble Mn^{2+} release ($[Mn^{2+}]$ = 1.3 mmol L^{-1}, after 24 h) represents only 3 % of the total Mn. Actually, the disproportionation of Mn^{III} according to reaction (1) should lead to the Mn^{2+} release in the solution and an increase in the corresponding Mn^{IV} content in the solid. From the observed Mn^{2+} release and the Mn AOS of the as prepared Na-birnessite equal to 3.65, the Mn AOS in the solid is expected to increase up to 3.68, while Mn AOS was measured equal to 4.00 for hexagonal birnessite. It should be noted that several reports mention also hexagonal birnessite with high Mn AOS up to 3.99 [5,29,41,53–56]. Then additional oxidative step should be considered.

Let us consider the reaction where Mn^{2+} undergoes oxidation to form additional Mn oxide (noted a-MnO_2):

$$Mn^{2+}_{(aq)} + ½\ O_{2(aq)} + H_2O_{(lq)} = a\text{-}MnO_{2(s)} + 2\ H^{+}_{(aq)} \quad (2)$$

Considering that activities of dissolved or ionic species are equal to their respective concentrations, activity of a-MnO_2 equal to 1 and taking the Henry's law constant for O_2 dissolution in water to be 7.92 10^4 kPa kg mol^{-1} [57], the chemical equilibrium constant of reaction (2) can be determined (with equation S1) and hence the corresponding standard Gibbs energy of reaction can be derived. Finally, from tabulated thermodynamics data of

aqueous Mn^{2+}, dissolved O_2, liquid H_2O and ionic H^+ (see Table 3), the standard Gibbs free energy of formation of the obtained Mn oxide can be calculated (with equation S3). The obtained value of $\Delta_f G°(a\text{-}MnO_2)$ is equal to -443.4 kJ mol^{-1}.

Interestingly, this value is lower to the one given for birnessite (δ-MnO_2) obtained by hausmannite oxidation in acidic medium $\Delta_f G°(\delta\text{-}MnO_2)$ = -452.8 kJ mol^{-1}[58] and also lower the one tabulated for most stable β-MnO_2 $\Delta_f G°(\beta\text{-}MnO_2)$ = -465.2 kJ mol^{-1}[59]. It is valuable to calculate the Mn^{2+} concentration at equilibrium when assuming δ-MnO_2 and β-MnO_2 formation, respectively. At pH = 3.5 and under atmospheric condition (298 K), the law of mass action gives a Mn^{2+} concentration equal to 30 µmol L^{-1} and to 0.2 µmol L^{-1}, respectively. It is necessary to point out that experimental analysis of the solution has given a much higher concentration of Mn^{2+}equal to 1.3 mmol L^{-1}.

After 24 h at pH = 3.5 in aerated conditions, triclinic Na-birnessite turns into a Na free hexagonal birnessite with Mn AOS equal to 4.00. Such birnessite is obtained from suspension with higher Mn^{2+} concentration than the one expected for β-MnO_2 particles suspension at the same pH. Considering that β-MnO_2 is the most stable MnO_2 phase, it appears that, in our case, birnessite was obtained from a solution presenting Mn^{2+} excess with respect to thermodynamic equilibrium. Therefore, reduced form of Mn can be anticipated at the near surface despite the high Mn AOS of bulk birnessite. This supposition is evidenced by XPS measurements where Mn^{II} and Mn^{III} were present. After acid treatment, the Mn AOS of the hexagonal birnessite at the surface was equal to ~ 3.6 (see Table 2) according to two different methods that correspond to the state of the art concerning Mn2p and Mn3p lines interpretation [21,25]. Similarly for triclinic Na-birnessite, the Mn AOS of the surface located in a range from 3.4 to 3.5 is lower than the Mn AOS of the bulk (3.65). The discrepancy between XPS and titration measurements may originate from the fact that XPS only probes the first few nm of the particles that are in the range of µm as determined from SEM measurements. One may

argue that manganese at the near-surface of birnessite is significantly more reduced than in the bulk. It should be noted that the O1s core-level spectra of birnessite evidenced appreciable amount of defects at the surface (O^- and OH moieties), which supports specific surface composition. Low Mn AOS at the surface can be attributed to the strong oxidative properties of Mn^{IV} as supposed in previous studies [21–24,56]. In contrast, Ilton *et al.* [25] performed angle resolve XPS measurements, from which they did not evidence any significant reduction of the top surface. However it may be argued that this discrepancy arises from the difficulty to carry out angle resolve XPS measurements on powder where particles are poorly oriented.

Table 3: Standard Gibbs free energies of formation of different species involved in studied reactions from [58,59].

Compound	$Mn^{2+}_{(aq)}$	β-$MnO_{2(s)}$	δ-$MnO_{2(s)}$	$H_2O_{(lq)}$	$O_{2(aq)}$
$\Delta_f G°$ (kJ mol^{-1})	-227.8	-465.2	-452.8	-237	16.3

5. Conclusion

The conversion of the triclinic birnessite into hexagonal one was monitored measuring the Mn amount in the liquid phase and a comprehensive set of solid characterization techniques. ICP, FTIR, Raman scattering and PXRD characterizations provide a consistent description of both solids. These investigations evidence the full transformation of single-phase triclinic Na-birnessite into hexagonal birnessite in acidic solution. Measurements in the far infrared range allow the identification absorption bands at 245 and 360 cm^{-1} for triclinic Na-birnessite and 341 cm^{-1} for hexagonal birnessite. It is worth noticing that the DFT cluster approach reported in previous works [26,27] predicted absorption bands at low wavenumber for hexagonal birnessite but no one was predicted for triclinic birnessite spectrum. To get a further insight into this band assignment, additional investigations by DFT should be performed with periodic boundary conditions allowing explicit description of the interlayer region and in particular of the Na^+ ion. To the best our knowledge, the first ^1H NMR signature of triclinic

and hexagonal birnessites is provided. ^{23}Na NMR measurements discriminated various chemical environments of sodium in triclinic birnessite, in particular NMR discriminate sodium close to Mn in the interlayer from sodium outside of the birnessite structure. This latter component was not detected by others techniques and clearly illustrated the relevance of a multi-technique approach in material study. The determination of the Mn^{II}, Mn^{III} and Mn^{IV} distribution on the surface based on the XPS $Mn2p_{3/2}$ and Mn3p features analyses gave similar results on both Na triclinic and hexagonal birnessites. In each case, surface AOS derived from XPS results were systematically lower than the AOS derived from bulk analysis. This leads us to recommend the determination of the surface AOS when birnessite reactivity is investigated.

Acknowledgements

We would like to acknowledge Pierrick Durand (Institut Jean Barriol, CRM2) for the PXRD characterizations, Claire Genois for the ICP-AES measurements (LCPME, Université de Lorraine, Villers les Nancy). We also thank Marc Hébrant for fruitful discussion and comments. We would like to thank the Tunisian Ministry of Higher Education and Scientific Research for the mobility grant accorded to Hella Boumaiza.

REFERENCES

[1] J.R. Bargar, C.C. Fuller, M.A. Marcus, A.J. Brearley, M. Perez De la Rosa, S.M. Webb, W.A. Caldwell, Structural characterization of terrestrial microbial Mn oxides from Pinal Creek, AZ, Geochim. Cosmochim. Acta. 73 (2009) 889–910. doi:10.1016/j.gca.2008.10.036.

[2] B. Lanson, V.A. Drits, Q. Feng, A. Manceau, Structure of synthetic Na-birnessite: Evidence for a triclinic one-layer unit cell, Am. Mineral. 87 (2002) 1662–1671. doi:10.2138/am-2002-11-1215.

[3] B. Lanson, V.A. Drits, E. Silvester, A. Manceau, Structure of H-exchanged hexagonal birnessite and its mechanism of formation from Na-rich monoclinic buserite at low pH, Am. Mineral. 85 (2000) 826–838. doi:10.2138/am-2000-5-625.

[4] J.E. Post, P.J. Heaney, J. Hanson, Rietveld refinement of a triclinic structure for synthetic Na-birnessite using synchrotron powder diffraction data, Powder Diffr. 17 (2002) 218–221. doi:10.1154/1.1498279.

[5] M. Villalobos, B. Toner, J. Bargar, G. Sposito, Characterization of the manganese oxide produced by Pseudomonas putida strain MnB1, Geochim. Cosmochim. Acta. 67 (2003) 2649–2662. doi:10.1016/S0016-7037(03)00217-5.

[6] E. Silvester, A. Manceau, V.A. Drits, Structure of synthetic monoclinic Na-rich birnessite and hexagonal birnessite: II. Results from chemical studies and EXAFS spectroscopy, Am. Mineral. 82 (1997) 962–978. doi:10.2138/am-1997-9-1013.

[7] J.E. Post, D.R. Veblen, Crystal structure determinations of synthetic sodium, magnesium, and potassium birnessite using TEM and the Rietveld method, Am. Mineral. 75 (1990) 477–489. papers2://publication/uuid/3EA72783-9E54-4EDC-935A-2A83ACF6716A.

[8] V.A. Drits, E. Silvester, A.I. Gorshkov, A. Manceau, Structure of synthetic monoclinic Na-rich birnessite and hexagonal birnessite: I. Results from X-ray diffraction and selected-area electron diffraction, Am. Mineral. 82 (1997) 946–961. doi:10.2138/am-1997-9-1012.

[9] D.C. Golden, Ion exchange, thermal transformations, and oxidizing properties of birnessite, Clays Clay Miner. 34 (1986) 511–520. doi:10.1346/CCMN.1986.0340503.

[10] W.T. Jiang, P.H. Chang, Y.S. Wang, Y. Tsai, J.S. Jean, Z. Li, Sorption and desorption of tetracycline on layered manganese dioxide birnessite, Int. J. Environ. Sci. Technol. 12 (2015) 1695–1704. doi:10.1007/s13762-014-0547-6.

[11] P. Le Goff, N. Baffier, S. Bach, J.P. Pereira-Ramos, Synthesis, ion exchange and electrochemical properties of lamellar phyllomanganates of the birnessite group, Mater. Res. Bull. 31 (1996) 63–75. doi:10.1016/0025-5408(95)00170-0.

[12] C.L. Peacock, D.M. Sherman, Sorption of Ni by birnessite: Equilibrium controls on Ni in seawater, Chem. Geol. 238 (2007) 94–106. doi:10.1016/j.chemgeo.2006.10.019.

[13] M.A. Rao, G. Iamarino, R. Scelza, F. Russo, L. Gianfreda, Oxidative transformation of aqueous phenolic mixtures by birnessite-mediated catalysis, Sci. Total Environ. 407 (2008) 438–446. doi:10.1016/j.scitotenv.2008.08.009.

[14] C.K. Remucal, M. Ginder-Vogel, A critical review of the reactivity of manganese oxides with organic contaminants, Environ. Sci. Process. Impacts. 16 (2014) 1247–1266. doi:10.1039/c3em00703k.

[15] R. Renuka, S. Ramamurthy, Investigation on layered birnessite type manganese oxides for battery applications, J. Power Sources. 87 (2000) 144–152. doi:10.1016/S0378-7753(99)00474-7.

[16] M.J. Scott, J.J. Morgan, Reactions at oxide surfaces. 2. Oxidation of Se(IV) by synthetic birnessite, Environ. Sci. Technol. 30 (1996) 1990–1996. doi:10.1021/es950741d.

[17] J.J. Lingane, R. Karplus, New Method for Determination of Manganese, Ind. Eng. Chem. - Anal. Ed. 18 (1946) 191–194. doi:10.1021/i560151a010.

[18] K.J. Vetter, N. Jaeger, Potentialausbildung an der Mangandioxid-Elektrode als oxidelektrode mit nichtstöchiometrischem oxid, Electrochim. Acta. 11 (1966) 401–419. doi:10.1016/0013-4686(66)80018-X.

[19] E. Chalmin, F. Farges, G.E. Brown, A pre-edge analysis of Mn K-edge XANES spectra to help determine the speciation of manganese in minerals and glasses, Contrib. to Mineral. Petrol. 157 (2009) 111–126. doi:10.1007/s00410-008-0323-z.

[20] A. Manceau, A.I. Gorshkov, V.A. Drits, Structural chemistry of Mn, Fe, Co, and Ni in manganese hydrous oxides: Part II. Information from EXAFS spectroscopy and

electron and X-ray diffraction, Am. Mineral. 77 (1992) 1144–1157.

[21] H.W. Nesbitt, D. Banerjee, Interpretation of XPS Mn(2p) spectra of Mn oxyhydroxides and constraints on the mechanism of MnO_2 precipitation, Am. Mineral. 83 (1998) 305–315. doi:10.2138/am-1998-3-414.

[22] H. Boumaiza, R. Coustel, G. Medjahdi, C. Ruby, L. Bergaoui, Conditions for the formation of pure birnessite during the oxidation of Mn(II) cations in aqueous alkaline medium, J. Solid State Chem. 248 (2017) 18–25. doi:10.1016/j.jssc.2017.01.014.

[23] I.G. McKendry, S.K. Kondaveeti, S.L. Shumlas, D.R. Strongin, M.J. Zdilla, Decoration of the layered manganese oxide birnessite with Mn(II/III) gives a new water oxidation catalyst with fifty-fold turnover number enhancement., Dalton Trans. 44 (2015) 12981–12984. doi:10.1039/c5dt01436k.

[24] H. Yin, W. Tan, L. Zheng, H. Cui, G. Qiu, F. Liu, X. Feng, Characterization of Ni-rich hexagonal birnessite and its geochemical effects on aqueous Pb^{2+}/Zn^{2+} and As(III), Geochim. Cosmochim. Acta. 93 (2012) 47–62. doi:10.1016/j.gca.2012.05.039.

[25] E.S. Ilton, J.E. Post, P.J. Heaney, F.T. Ling, S.N. Kerisit, XPS determination of Mn oxidation states in Mn (hydr)oxides, Appl. Surf. Sci. 366 (2016) 475–485. doi:10.1016/j.apsusc.2015.12.159.

[26] E.A. Johnson, J.E. Post, Water in the interlayer region of birnessite: Importance in cation exchange and structural stability, Am. Mineral. 91 (2006) 609–618. doi:10.2138/am.2006.2090.

[27] F.T. Ling, J.E. Post, P.J. Heaney, J.D. Kubicki, C.M. Santelli, Fourier-transform infrared spectroscopy (FTIR) analysis of triclinic and hexagonal birnessites, Spectrochim. Acta - Part A Mol. Biomol. Spectrosc. 178 (2017) 32–46. doi:10.1016/j.saa.2017.01.032.

[28] Y.K. Hsu, Y.C. Chen, Y.G. Lin, L.C. Chen, K.H. Chen, Reversible phase transformation of MnO_2 nanosheets in an electrochemical capacitor investigated by in situ Raman spectroscopy, Chem. Commun. 47 (2011) 1252–1254. doi:10.1039/c0cc03902k.

[29] H. Zhao, M. Zhu, W. Li, E.J. Elzinga, M. Villalobos, F. Liu, J. Zhang, X. Feng, D.L. Sparks, Redox reactions between Mn(II) and hexagonal birnessite change its layer

symmetry, Environ. Sci. Technol. 50 (2016) 1750–1758. doi:10.1021/acs.est.5b04436.

[30] K.A. Aldi, J. Cabana, P.J. Sideris, C.P. Grey, Investigation of cation ordering in triclinic sodium birnessite via ^{23}Na MAS NMR spectroscopy, Am. Mineral. 97 (2012) 883–889. doi:10.2138/am.2012.3933.

[31] AFNOR NF X 31-130, Détermination de la capacité d'échange cationique (CEC) et des cations extractibles. Qualité des sols, Volume 1, Assoc. Française Norm. Paris, Fr. 1999. (n.d.) 265–278.

[32] A. Gaillot, Caractérisation structurale de la birnessite (Ph.D. Thesis), University of Grenoble, France, 2002.

[33] W.J. Langston, Bebianno, M. J., Metal Metabolism in Aquatic Environments, 1998. doi:10.1007/978-1-4757-2761-6.

[34] G. Davies, Some aspects of the chemistry of manganese(III) in aqueous solution, Coord. Chem. Rev. 4 (1969) 199–224. doi:10.1016/S0010-8545(00)80086-7.

[35] R. Ma, Y. Bando, L. Zhang, T. Sasaki, Layered MnO_2 nanobelts: Hydrothermal synthesis and electrochemical measurements, Adv. Mater. 16 (2004) 918–922. doi:10.1002/adma.200306592.

[36] H.T. Zhang, X.H. Chen, J.H. Zhang, G.Y. Wang, S.Y. Zhang, Y.Z. Long, Z.J. Chen, N.L. Wang, Synthesis and characterization of one-dimensional $K_{0.27}MnO_2 \cdot 0.5H_2O$, J. Cryst. Growth. 280 (2005) 292–299. doi:10.1016/j.jcrysgro.2005.02.063.

[37] H.T. Zhu, J. Luo, H.X. Yang, J.K. Liang, G.H. Rao, J.B. Li, Z.M. Du, Birnessite-type MnO_2 nanowalls and their magnetic properties, J. Phys. Chem. C. 112 (2008) 17089–17094. doi:10.1021/jp804673n.

[38] A.C. Larson, R.B. Von Dreele, General Structure Analysis System (GSAS), Los Alamos - USA, 1994.

[39] B.H. Toby, EXPGUI, a graphical user interface for GSAS, J. Appl. Crystallogr. (2001) 210–213. doi:10.1017/CBO9781107415324.004.

[40] H. Cui, G. Qiu, X. Feng, W. Tan, F. Liu, Birnessites with different average manganese oxidation states synthesized, characterized, and transformed to todorokite at atmospheric pressure, Clays Clay Miner. 57 (2009) 715–724.

doi:10.1346/CCMN.2009.0570605.

[41] X. Feng, Pathways of birnessite formation in alkali medium, Sci. China Ser. D. 48 (2005) 1438. doi:10.1360/03yd0280.

[42] R.M. Potter, G.R. Rossman, Mineralogy of manganese dendrites and coatings, Am. Mineral. 64 (1979) 1219-1226. http://www.minsocam.org/ammin/AM64/AM64_1199.pdf?ref=PandoraISP.

[43] A. Bayoudh, N. Etteyeb, R. Kossai, Hydrothermal synthesis, characterization and electrochemical properties of γ-MnOOH nanobelts, Ceram. Int. 41 (2014) 12273–12279. doi:10.1016/j.ceramint.2015.06.051.

[44] M. Ocaña, Uniform particles of manganese compounds obtained by forced hydrolysis of manganese(II) acetate, Colloid Polym. Sci. 278 (2000) 443–449. doi:10.1007/s003960050537.

[45] C. Julien, M. Massot, R. Baddour-Hadjean, S. Franger, S. Bach, J.P. Pereira-Ramos, Raman spectra of birnessite manganese dioxides, Solid State Ionics. 159 (2003) 345–356. doi:10.1016/S0167-2738(03)00035-3.

[46] L. Yang, S. Cheng, X. Ji, Y. Jiang, J. Zhou, M. Liu, Investigations into the origin of pseudocapacitive behavior of Mn_3O_4 electrodes using in operando Raman spectroscopy, J. Mater. Chem. A. 3 (2015) 7338–7344. doi:10.1039/c5ta00223k.

[47] C. Julien, M. Massot, Spectroscopic studies of the local structure in positive electrodes for lithium batteries, Phys. Chem. Chem. Phys. 4 (2002) 4226–4235. doi:10.1039/b203361e.

[48] Z. Morgan Chan, D.A. Kitchaev, J. Nelson Weker, C. Schnedermann, K. Lim, G. Ceder, W. Tumas, M.F. Toney, D.G. Nocera, Electrochemical trapping of metastable Mn^{3+} ions for activation of MnO_2 oxygen evolution catalysts, Proc. Natl. Acad. Sci. 115 (2018) E5261–E5268. doi:10.1073/pnas.1722235115.

[49] A.Y. Nosaka, E. Kojima, T. Fujiwara, H. Yagi, H. Akutsu, Y. Nosaka, Photoinduced Changes of Adsorbed Water on a TiO_2 Photocatalytic Film As Studied by ^{1}H NMR Spectroscopy, J. Phys. Chem. B. 107 (2003) 12042–12044. doi:10.1021/jp035526v.

[50] V.P. Santos, M.F.R. Pereira, J.J.M. Órfão, J.L. Figueiredo, The role of lattice oxygen on the activity of manganese oxides towards the oxidation of volatile organic

compounds, Appl. Catal. B Environ. 99 (2010) 353–363. doi:10.1016/j.apcatb.2010.07.007.

[51] N.H. Wang, S.L. Lo, Preparation, characterization and adsorption performance of cetyltrimethylammonium modified birnessite, Appl. Surf. Sci. 299 (2014) 123–130. doi:10.1016/j.apsusc.2014.01.195.

[52] R.P. Gupta, S.K. Sen, Calculation of multiplet structure of core p-vacancy levels. II, Phys. Rev. B. 12 (1975) 15–19. doi:10.1103/PhysRevB.12.15.

[53] X.H. Feng, L.M. Zhai, W.F. Tan, F. Liu, J.Z. He, Adsorption and redox reactions of heavy metals on synthesized Mn oxide minerals, Environ. Pollut. 147 (2007) 366–373. doi:10.1016/j.envpol.2006.05.028.

[54] T. Gao, Y. Shen, Z. Jia, G. Qiu, F. Liu, Y. Zhang, X. Feng, C. Cai, Interaction mechanisms and kinetics of ferrous ion and hexagonal birnessite in aqueous systems, Geochem. Trans. 16 (2015) 16. doi:10.1186/s12932-015-0031-3.

[55] Y. Wang, X. Feng, M. Villalobos, W. Tan, F. Liu, Sorption behavior of heavy metals on birnessite: Relationship with its Mn average oxidation state and implications for types of sorption sites, Chem. Geol. 292–293 (2012) 25–34. doi:10.1016/j.chemgeo.2011.11.001.

[56] Q. Ye, H. Lu, J. Zhao, S. Cheng, T. Kang, D. Wang, H. Dai, A comparative investigation on catalytic oxidation of CO, benzene, and toluene over birnessites derived from different routes, Appl. Surf. Sci. 317 (2014) 892–901. doi:10.1016/j.apsusc.2014.08.126.

[57] E.A. Moelwyn-Hughes, D. Lewis, Physical Chemistry, J. Electrochem. Soc. 1960 volume 107, issue 5, 1960. doi:10.1149/1.2427699.

[58] O. Bricker, Some stability relations in the system Mn-O_2-H_2O at 25° and one atmosphere total pressure, Am. Mineral. 50 (1965) 1296–1354.

[59] N. Lange, J.A. Dean, Handbook of Chemistry., McGraw-Hil, New York (N.Y.), 1999. doi:10.1080/10426919008953291.

$Mn2p_{3/2}$and Mn3p XPS spectra of triclinic Na-birnessite and hexagonal birnessite

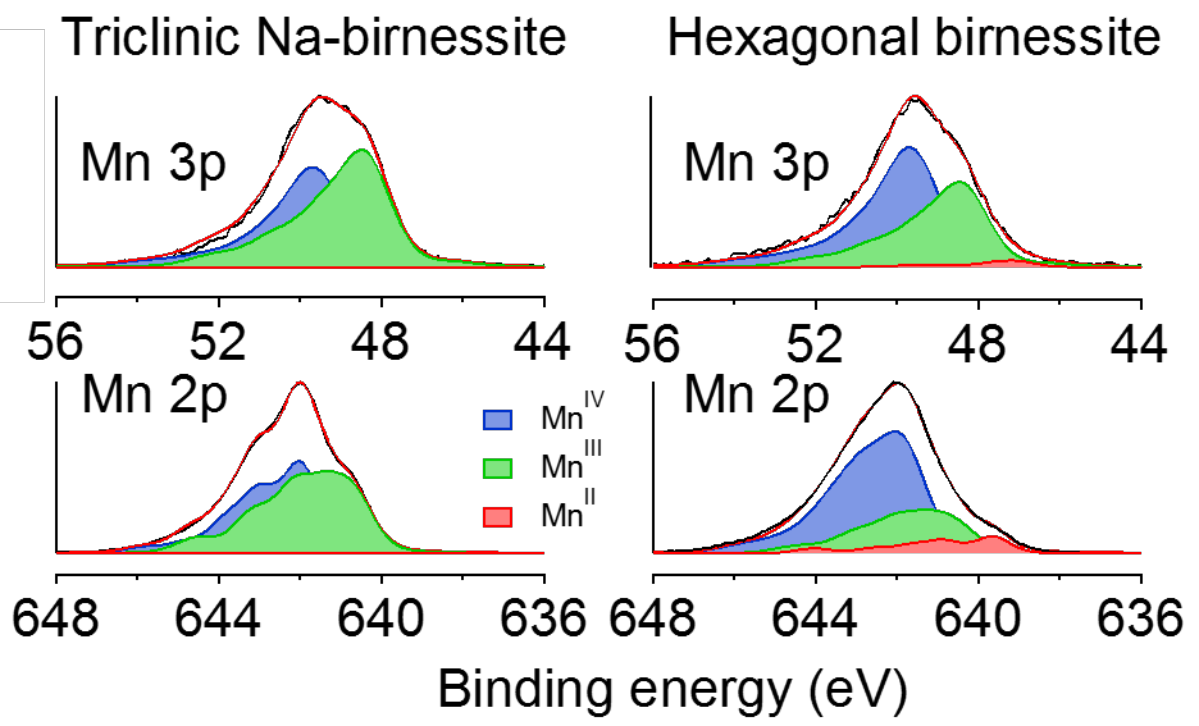
Triclinic Na-birnessite
Hexagonal birnessite
Mn 3p
Mn 3p
56
52
48
44
56
52
48
44
Mn 2p
Mn 2p
Mn^{IV}
Mn^{III}
Mn^{II}
648
644
640
636
648
644
640
636
Binding energy (eV)